Structural Characterization of the Partially Folded Intermediates of an Immunoglobulin Light Chain Leading to Amyloid Fibrillation and Amorphous Aggregation†

Zhijie Qin, Dongmei Hu, Min Zhu, and Anthony L. Fink*

Department of Chemistry & Biochemistry, University of California, Santa Cruz, California 95064

Received August 22, 2006; Revised Manuscript Received December 11, 2006

ABSTRACT: Immunoglobulin light chain deposition diseases involve various types of extracellular deposition of light chain variable domains, including amyloid fibrils and amorphous deposits. The decreased thermodynamic stability of the light chain is believed to be the major factor leading to fibrillation. However, the differences in the nature of the deposits among the light chain deposition diseases raise the question of whether the mechanisms leading to fibrillar or amorphous aggregation is different. In this study, we generated two partially folded intermediates of the light chain variable domain SMA in the presence of guanidine hydrochloride (GuHCl) and characterized their conformations. The more unfolded intermediate formed fibrils most rapidly, while the more native-like intermediate predominantly led to amorphous deposits. The results also show that the monomeric, rather than the dimeric state, was critical for fibrillation. The data also indicate that fibril elongation involves addition of a partially unfolded intermediate, rather than the native state. We postulate that a more highly unfolded intermediate is more suited to undergo the topological rearrangements necessary to form amyloid fibrils than a more structured one and that this also correlates with increased destabilization. In the case of light chain aggregation, it appears that more native-like intermediate conformations are more prone to form amorphous deposits.

Light chain deposition diseases involve the extracellular deposition of amyloid fibrils and other forms of immunoglobulin light chain variable domains (V_L)[1] (*1*, *2*). The features of the protein deposited in tissues vary within the different light-chain-related deposition diseases. In AL or primary amyloidosis, the most common systemic amyloidosis, the deposits are in the form of amyloid fibrils, most commonly in the kidney and heart. In light-chain deposition disease (LCDD), the amorphous deposits are found associated with basement membranes (*3*, *4*). Occasionally, patients may present with both AL amyloidosis and LCDD, both comprised of same V_L and sometimes in the same tissue (*5*). The molecular mechanisms of how the immunoglobulin light chains form amyloid are still unclear, in particular, why some immunoglobulin light chains form amyloid and others form amorphous deposits. Although some models assume that aggregate/amyloid formation occurs essentially from the native conformation (*5*−*7*), more and more evidence suggests that decreased thermodynamic stability of the light chain, leading to a population of partially folded intermediates, is the major factor in amyloidosis (*8*−*10*). Our previous studies on light chain fibrillation have shown that the fibrils arise from the formation of partially folded intermediates, association of these leads to formation of soluble oligomers and the critical fibrillation nucleus, and subsequently the initial fibrillar species, typically, a protofilament or protofibril, and finally these associate into mature fibrils (*8*, *11*−*14*). In addition, the factors that determine the particular location of the deposits and whether they will be fibrillar or amorphous (as in LCDD) are unknown. Although the deposits are usually extracellular, there is also controversy as to whether they are initially formed intracellularly, e.g., in lysosomes, or extracellularly (*15*).

The V_L domain used in this study is named SMA (114 residues, $M_r = 12\,700$), the variable domain of a recombinant amyloidogenic light chain engineered by Stevens et al. (*16*), which was initially extracted from lymph node-derived amyloid fibrils of an AL amyloidosis patient (*17*). Its sequence is very similar to that of the light chain domain, LEN, which was derived from a patient with multiple myeloma who showed no evidence of renal dysfunction or amyloidosis (*18*). The sequences of SMA and LEN are very similar, differing only at eight positions out of 114. Four of these are in CDR3 (Q89H, T94H, Y96Q, S97T), two are in CDR1 (S29N, K30R), and the remaining two are in the framework region (P40L, I106L). The high-resolution crystallographic structure of LEN (1.8 Å) has been solved (PDB Accession No. 1LVE) (*19*). Both SMA and LEN belong to the *k*IV family of immunoglobulins.

Previously, we have shown that decreasing the pH to around pH 5 leads to formation of a native-like partially unfolded intermediate and formation of amorphous deposits, whereas decreasing the pH to around pH 2 leads to formation of a significantly more unfolded intermediate and formation of amyloid fibrils (*8*). In this study, we confirm that mildly

† This research was supported by a grant from the National Institutes of Health (DK55675).

* Corresponding author. E-mail: enzyme@ucsc.edu. Phone: (831) 459-2744. Fax: (831) 459-2935.

[1] Abbreviations: GuHCl, guanidinium hydrochloride; CDR, complementary determining region; ANS, 1-anilino-8-naphthalene sulfonic acid; ThT, thioflavin T; V_L, light chain variable domain.

10.1021/bi061716v CCC: $37.00
Published on Web 02/22/2007

destabilizing conditions lead to a native-like partially unfolded conformation, whereas more strongly destabilizing conditions lead to a more unfolded intermediate and formation of fibrils. Thus, this generality could explain the nature of the deposits (fibrillar or amorphous). Using guanidine hydrochloride (GuHCl) to destabilize SMA, two partially folded intermediate conformations were detected, with maximum populations around 1 and 2 M GuHCl, respectively. The conformations and aggregation properties were characterized. The unfolded intermediate preferentially gave fibrils, while the native-like intermediate preferentially led to amorphous aggregation. Fibrillation was much slower for the dimeric form of SMA, suggesting that the monomer, rather than the dimer, was the critical species for fibrillation.

MATERIALS AND METHODS

Chemicals. GuHCl was purchased from EM Science. Peptone and yeast extract used in the medium were purchased from Difco. All other chemicals were purchased from Fisher or Sigma and were of the highest grade available. The water was doubly deionized.

Expression and Purification of Recombinant SMA. The recombinant V_L domain SMA was purified from JM83 *Escherichia coli* cells transformed with the plasmid pkIVsma004, generously provided by Dr. Fred Stevens, Argonne National Lab (*16*). The overexpressed protein was purified using the procedure of Stevens et al. (*16*) with minor modifications. Briefly, the recombinant protein was extracted from the periplasm using osmotic shock via treatment with ice-cold extraction buffer (0.2 M Tris, 0.5 mM EDTA, 0.5 M sucrose, pH 7.5) followed by distilled water. The periplasmic extract was dialyzed against four changes of 20 volumes of 10 mM acetate buffer, pH 5.6, and loaded onto a fast-flow SP Sepharose column (Pharmacia). The column was washed with 10 mM acetate buffer, pH 5.6, and the protein was eluted using 10 mM phosphate buffer, pH 8.0. The fractions were assayed by SDS−PAGE, and fractions containing the recombinant protein were pooled, concentrated by ultrafiltration with a molecule cutoff of 3000 Da (Amicon), followed by a size exclusion column of Sephacryl 200 (Pharmacia) for further purification. The purified protein was stored in glass vials in 10 mM phosphate buffer (pH 8.0) at 4 °C and used within 2 months of the initial purification. Protein concentrations were measured via optical density at 280 nm using the extinction coefficient of $E_{0.1\%} = 1.71$ calculated from the sequence. The purity of the protein preparations was assayed by SDS−PAGE and electrospray mass spectrometry (positive ionization).

Circular Dichroism Spectra Collection. CD spectra were collected on an AVIV model 62DS spectrometer between 250 and 200 nm for the far-UV region and between 320 and 250 nm for the near-UV region, with a step size of 1.0 nm and an averaging time of 1 s and collecting five repeat scans. Cells of 1 to 0.01 cm path length were used for far- and 0.4 to 10 cm for near-UV CD measurements with protein concentrations of 240 to 24 μM, respectively. All the samples with GuHCl were incubated at 25 °C for at least 40 min to reach equilibration of the unfolding reaction (experiments measuring the kinetics of unfolding demonstrated that equilibration was reached prior to the CD measurements). The background from the buffers was subtracted, and the data were converted into mean residual weight ellipticity (MRW) according to their concentrations and path lengths.

Intrinsic Tryptophan Fluorescence Measurements. Fluorescence measurements were made with a FluoroMax-2 fluorescence spectrometer (Jobin Yvon-Spex). Emission spectra between 305 and 450 nm were collected with excitation at 295 nm and a 1 nm band-pass. The samples of SMA (16 μM) were incubated in 10 mM phosphate buffer (pH 7.4), 200 mM NaCl containing varying amounts of GuHCl (0−6 M) for at least 40 min at 25 °C to ensure equilibration of the unfolding reaction (confirmed by kinetics measurements). Data of fluorescence intensity and the emission λ_{max} were analyzed by nonlinear least-squares fitting to a three-state folding model. The fraction unfolded, F_u, was calculated using the equation:

$$F_u = (y_f - y)/(y_f - y_u) \quad (1)$$

where y represents the observed fluorescence at a particular concentration of GuHCl, and y_f and y_u represent the corresponding fluorescence emission at the λ_{max} of the folded and unfolded states, respectively, at that GuHCl concentration.

ANS-Binding Fluorescence Measurements. 1-Anilino-8-naphthalene sulfonic acid (ANS) fluorescence measurements were performed using an excitation wavelength of 380 nm and recording the emission spectra from 420 to 600 nm (1 nm band-pass). The protein (8 μM) was first incubated with various concentrations of GuHCl in 10 mM phosphate buffer (pH 7.4) at 25 °C for 20 min to attain unfolding equilibrium. ANS was then added to a concentration of 4 μM, and the fluorescence spectra were collected on a FluoroMax-3 fluorescence spectrometer at 25 °C (this concentration of ANS was found to be optimal). ANS fluorescence intensities and emission maximum wavelength were plotted versus GuHCl concentrations.

Fluorescence Anisotropy Measurements. Samples of 16 μM protein were prepared in various concentrations of GuHCl for static unfolding measurements, and with a series of protein concentrations (8−240 μM) in 2 M GuHCl to monitor the dissociation of dimers. All samples were incubated at 25 °C for at least 40 min, and then the anisotropies were measured on the FluoroMax-3 fluorescence spectrometer with polarizers, with excitation wavelength of 295 nm (1 nm band-pass) and the emission wavelength of 352 nm (1 nm band-pass) and 1 mm path length.

Acrylamide Quenching. Quenching experiments were performed by following the intrinsic fluorescence intensity of SMA solution (16 μM) upon adding a series of 5 μL aliquots of a 3.0 M acrylamide solution. The measurements used an excitation wavelength of 295 nm (1 nm band-pass), and the emission spectra were collected from 300 to 420 nm (1 nm band-pass). Fluorescence intensities were further corrected for dilution due to the stepwise addition of acrylamide. The data were plotted as the ratio of the fluorescence intensity in the absence of acrylamide (F_o) to the fluorescence intensity in the presence of acrylamide (F) versus the concentration of acrylamide ([A]). The values of the Stern−Volmer constant (K_{SV}) or dynamic quenching constant (K_{ST}) were obtained by curve-fitting the experimental data to eq 2:

$$F_0/F = (1 + K_{SV}[A]) \times \exp(K_{ST}[A]) \quad (2)$$

where K_{ST} represents the static quenching constant responsible for a slight upward curvature.

SAXS Measurements. Small-angle X-ray scattering measurements were performed on Beam line 4−2 at the Stanford Synchrotron Radiation Laboratory (SSRL) as described previously (*20*). The SAXS instrument was configured with a Mo:CB_4 multilayer monochromator, an 18 mm beamstop, and a 218 cm sample-to-detector distance. The samples were prepared into various concentrations of GuHCl in 10 mM phosphate buffer, pH 7.4. After incubation at 25 °C for 30 min, the samples were illuminated to the beam using a PTFE flow-cell with 1.3 mm path length to minimize radiation damage. Data were collected with the accumulating time of 10 min at 25 °C. Buffer was subtracted and radii of gyration were calculated using the Guinier approximation (*21*).

In Vitro Fibril Formation Assays. Fibril formation was monitored using a fluorescence assay based on the enhanced fluorescence of the dye thioflavin T (ThT) on binding to amyloid fibrils (*12*). Samples of purified protein in 10 mM phosphate buffer pH 7.4 and 200 mM NaCl were incubated either in 96-well plates or vials for manual assay. Prior to starting the incubation, the protein was ultracentrifuged at 178000*g* on an Airfuge (Beckman) for 30 min to eliminate any aggregated material. In the plate reader assay, the solutions contained protein at the indicated concentrations and other additives as indicated, as well as 5 μM ThT. A volume of 150 μL of the mixture was pipetted into the well of a 96-well plate (white plastic, clear bottom), and a 3 mm diameter glass sphere (Fisher) was added. Each sample was run in quadruplicate or sextuplicate. The plates were sealed with Mylar plate sealers (Dynex) and loaded into a fluorescence plate reader (Fluoroskan Ascent), incubated at 37 °C with shaking at 600 rpm with a shaking diameter of 1 mm. The samples were shaken to speed the rate of fibril formation. The fluorescence was measured at 30 min intervals with excitation at 444 nm and emission at 485 nm, with a sampling time of 40 ms.

In the manual assay, the protein sample was incubated under the desired conditions (as above) in a 1.8 mL flat-bottomed screw-capped glass vial with moderate stirring using a Teflon-coated microstir bar. Typical fibril growth experiments involved incubating the protein at 37 °C with constant stirring and removing aliquots (10 μL) over time for analysis by light scattering and ThT binding (see below). Constant temperatures were maintained using a circulating water bath. At each time point, a 220 μL sample was removed and transferred to a cylindrical quartz microcell to measure Rayleigh light scattering at 600 nm with a 1 nm band-pass for both excitation and emission monochromators. Thioflavin T binding assays were conducted by adding sample aliquots (10 μL) to 990 μL of 20 μM ThT in 10 mM phosphate buffer, pH 7.4, in a 1 mL fluorescence cuvette. Fluorescence emission was monitored with excitation at 450 nm using a 1 nm band-pass on both the excitation and emission monochromators. Fluorescence intensities were reported at 482 nm.

The data were fit to a sigmoidal equation (eq 3) using Sigmaplot:

$$F = (F_i + m_i t) \pm (F_f + m_f t)/(1 + \exp(t - t_m)/\tau) \quad (3)$$

where F is the fluorescence intensity and t_m is the time to 50% of maximal fluorescence. The initial baseline during the lag time is described by $F_i + m_i t$. The final baseline after the growth phase has ended is described by $F_f + m_f t$. The apparent rate constant, k_{app}, for the growth of fibrils is given by $1/\tau$, the lag time is calculated as $t_m - 2\tau$, and the amplitude, amp, is given by $F_f - F_i$. Although eq 1 gave very good fits for the ThT kinetic profiles, the expression is strictly a simple empirical means of providing kinetic parameters for comparing rates of fibrillation from different samples and does not directly reflect the underlying complex kinetic scheme.

Transmission Electron Microscopy (EM). The aggregates of SMA were checked by EM. The stirred protein solutions were sampled at predetermined time points during the kinetic experiments by dropping 10 μL protein samples on Formvar-coated copper grids. After the excess sample was drained with filter paper, the grids were rinsed three times with water and air-dried. A freshly prepared 2% (w/v) uranyl acetate solution was then applied on the grids for 5 min. After the excess negative staining solution was removed, the grids were air-dried again. Electron micrographs were collected using a JEOL JEM-100B microscope with a voltage accelerator of 80 kV. A magnification of 75 000 was used.

RESULTS

Partially Folded Conformations of SMA. The effect of destabilizing the conformation of SMA was investigated by adding increasing amounts of GuHCl at pH 7.4, and the resulting conformations were monitored by means of near- and far-UV CD, intrinsic Trp fluorescence, ANS-binding fluorescence, acrylamide quenching, fluorescence anisotropy, and small-angle X-ray scattering.

The far-UV CD spectra of SMA were recorded at 80 μM in the presence of various concentrations of GuHCl (Figure 1a). The spectrum of native SMA (pH 7.4) was characterized by two minima at 219 and 232 nm. The minimum at 219 nm reflects the predominant β structure of the protein (*19*), and the minimum at 232 nm is due to the presence of aromatic clusters (*22*). With the addition of increasing concentration of GuHCl up to 1 M, both of the minima become significantly decreased, indicating the loss of significant amounts of secondary structure. Upon increasing the concentration of GuHCl above 1 M, the trough at 219 nm shifted to 215 nm reaching a minimum at 2 M GuHCl, while the minimum at 232 nm became progressively more shallow, reflecting a rearrangement of the structure to a β-rich conformation with a loose tertiary structure. With GuHCl concentrations above 2 M, the minimum at 215 nm decreased progressively but did not disappear even in the presence of 5.5 M GuHCl, indicating the existence of some residual secondary structure. Plotting the ellipticity at 217 nm against GuHCl, Figure 1b, reveals two transitions corresponding to two intermediates: at 1 and 2 M GuHCl, respectively. The corresponding far-UV CD spectra (Figure 1a) indicate significant changes in structure for both of these intermediates.

Information about the effects of GuHCl on the tertiary structure of SMA and its intermediates was obtained from their near-UV CD spectra: Under native conditions (pH 7.4, 0 M GuHCl) the spectrum was characterized by several maxima (Figure 1c, inset). In the presence of 1 M GuHCl,

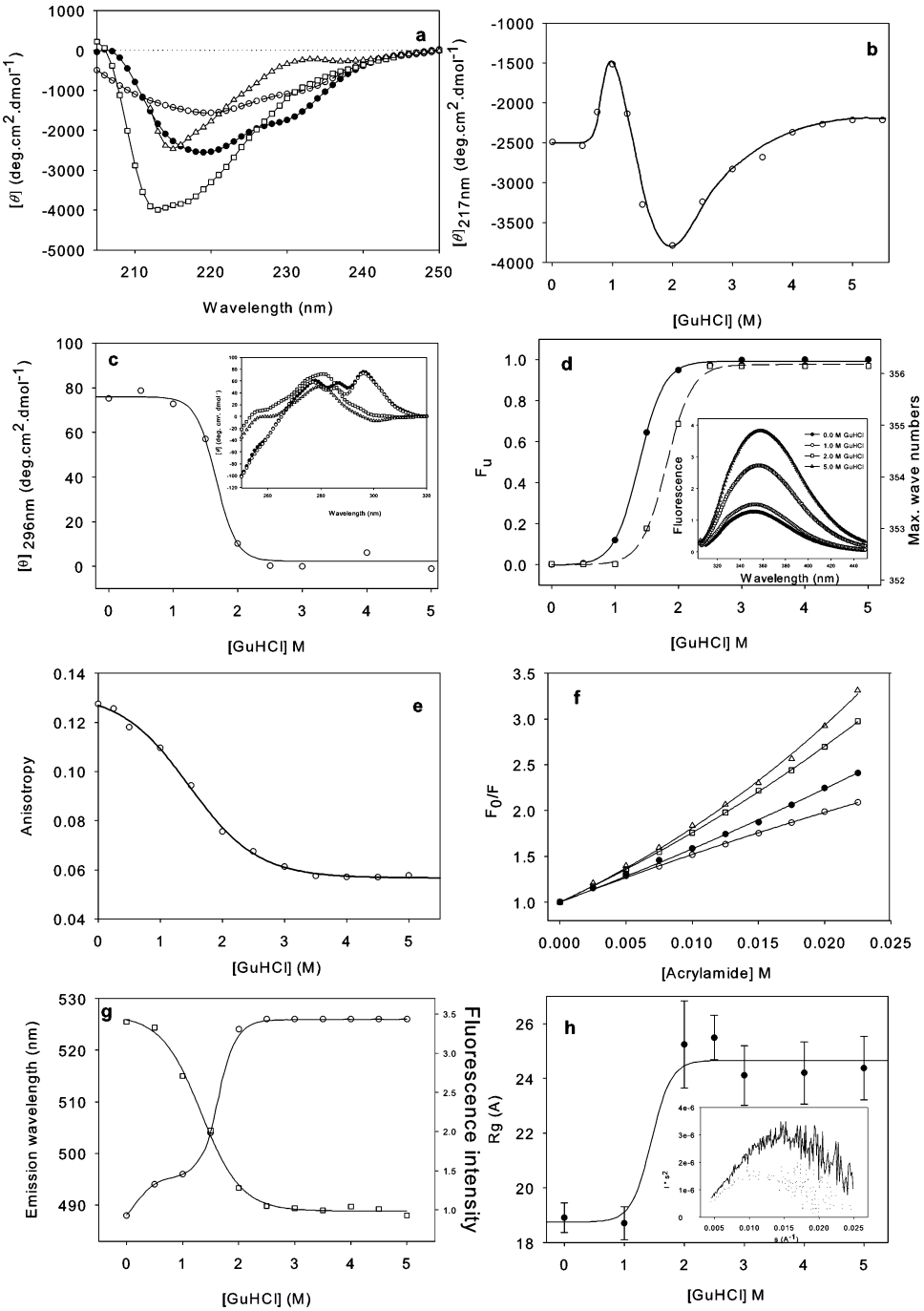

FIGURE 1: Conformational properties of SMA at pH 7.4 (10 mM phosphate buffer and 200 mM NaCl) induced by various concentrations of GuHCl and assessed by different techniques. (a) Far-UV circular dichroism spectra of SMA; native state (●), 1 M GuHCl (○), 2 M GuHCl (□), and 5.5 M GuHCl (△). (b) Conformational transitions of SMA as a function of GuHCl probed by far-UV CD at 217 nm. (c) Conformational transitions of SMA as a function of GuHCl monitored by near-UV CD at 296 nm. The inset shows the spectra of native SMA (●), with 1 M GuHCl (○), 2 M GuHCl (□), and 5 M GuHCl (△). (d) Conformational transitions of SMA as a function of GuHCl from intrinsic tryptophan fluorescence spectra, 8 μM SMA. The solid circles represent the maximum emission wavelength; the open squares represent the fluorescence intensity. The inset shows the spectra of SMA in the presence of GuHCl at 0 M (●), 1 M (○), 2 M (□), and 5.5 M (△). (e) Fluorescence anisotropy of SMA for different concentrations of GuHCl. (f) Stern−Volmer plots of acrylamide quenching of the tryptophan fluorescence of SMA (8 μM) in the presence of 0 M (●), 1 M (○), 2 M (□), and 5.0 M (△) GuHCl. (g) ANS fluorescence intensity (□) and the emission wavelength (○) for 8 μM SMA in the presence of various concentrations of GuHCl. (h) Radius of gyration of SMA in the presence of various concentrations of GuHCl calculated from small-angle X-ray scattering profiles at a SMA concentration of 240 μM. The inset shows the Kratky plots of SMA in its native state (solid line) and with 2 M GuHCl (dotted line).

the spectrum was not significantly changed, but there was a small decrease in intensity in the vicinity of the peak at 285 nm, indicating that the intermediate at 1 M GuHCl possesses a similar tertiary structure to the native conformation. Upon increasing the GuHCl concentration to 2 M, a significant decrease of the intensities of the two maxima at 296 and 285 nm and an increase in the maximum at 280 nm was observed, suggesting a significant difference in the tertiary structure of the second intermediate from the native state and the first intermediate. The maximum at 280 nm was, however, still observed in the spectrum obtained for the sample containing 5 M GuHCl, indicating that residual

structure was still present under these conditions, most likely the aromatic cluster.

The two tryptophan residues at positions 35 and 50 provide a probe to detect changes in their environment by monitoring the intrinsic fluorescence excited at 295 nm. Whereas Trp^{35} is buried in the hydrophobic core of the protein, Trp^{50} is significantly solvent-exposed by comparison with LEN (*19*). However, in the native state the fluorescence contribution of Trp^{35} is completely quenched by the spatial proximity of the disulfide bridge. Thus, under native conditions, the intrinsic fluorescence of SMA results from the solvent-exposed Trp^{50}, as illustrated by the high λ_{max} value of 352 nm at pH 7.4 in the absence of GuHCl (Figure 1d, inset). With increasing concentrations of GuHCl above 1 M, the fluorescence intensity significantly increased to a maximum at 3 M GuHCl accompanied by a shift in the λ_{max} from 352 to 358 nm. These changes indicate that Trp^{35}, buried in the hydrophobic core of the protein in its native state, moves away from the disulfide bridge and becomes solvent-exposed. The spectra indicate that in the intermediate at 1 M GuHCl the environment of the buried Trp is similar to that in the native state, whereas there have been significant changes in the structure of the intermediate at 2 M GuHCl, allowing the formerly buried Trp to become significantly solvent exposed.

Fluorescence anisotropy can provide information about molecular size and fluorophore flexibility. As shown in Figure 1e, a small decrease in anisotropy was observed as the GuHCl concentration increased to 1 M. A more significant decrease was seen as the GuHCl concentration increased to 3 M. At the protein concentration used in these experiments, SMA will be predominantly monomeric (see below). Thus, changes in the anisotropy will reflect either differences in the size of the monomer or changes in the mobility of the Trps. Since a decrease in size of the protein under these conditions is difficult to conceive, we attribute the observed decrease in anisotropy with increased GuHCl to increased flexibility of the molecular framework, allowing increased motion of the Trps, in particular, the formerly buried Trp^{35}.

ANS fluorescence has been used to probe protein conformational changes associated with the solvent exposure of hydrophobic regions (*23*−*25*), usually observed upon partial protein unfolding (e.g., the molten globule state). Both an increase in fluorescence intensity and a decrease in λ_{max} (blue shift) are usually observed upon binding of ANS to exposed, Figure 1d hydrophobic regions. ANS binding experiments with SMA solutions at pH 7.4 and various amounts of GuHCl were performed using ANS solution to detect possible partially unfolded intermediates. In contrast to most proteins, SMA can bind ANS in its native state based on the λ_{max} value of 488 nm and higher fluorescence intensity than that of the ANS control (no protein) (data not shown). Upon adding increasing concentrations of GuHCl to 2.5 M, the λ_{max} red-shifted from 488 to 526 nm, accompanied by a decrease in fluorescence intensity Figure 1g, indicating dissociation of ANS from an ANS−protein complex as unfolding occurred with higher concentrations of GuHCl. Significantly a minor transition is observed around 1 M GuHCl in the λ_{max} curve, which presumably reflects the intermediate existing in 1 M GuHCl as shown in the CD data.

Table 1: Stern−Volmer Constants for Trp Accessibility of SMA in the Presence of Various Concentrations of GuHCl from Acrylamide Quenching Measurements

[GuHCl] (M)	K_{SV} (M^{-1})	K_{ST} (M^{-1})
0	50.88 ± 3.20	4.60 ± 1.65
1	49.74 ± 0.53	0.00 ± 1.70
2	55.37 ± 0.94	12.43 ± 0.47
5	56.13 ± 0.59	15.56 ± 2.44

Acrylamide quenching experiments were performed on SMA solutions (8 μM) and pH 7.4 with increasing amounts of GuHCl (from 0 to 5 M) Figure 1f. The upward curvature in the Stern−Volmer plots indicates the presence of static quenching (direct interactions in the ground state between acrylamide and the fluorophores), while the Stern−Volmer constants (K_{SV}) account for the kinetic quenching due to the interaction of the quencher with the excited-state of the fluorophores. As shown in Figure 1f and Table 1, both K_{ST} and K_{SV} obtained from curve fitting the data for solutions containing 0−5 M GuHCl were different, and increased with increasing concentration of GuHCl, indicating increased solvent accessibility of the Trps. The value for K_{SV} at 2 M GuHCl is similar to that of 5 M GuHCl, suggesting near-maximum solvent accessibility of the buried Trp already in the intermediate at 2 M GuHCl. However, K_{SV} of SMA in 1 M GuHCl is smaller than that at higher GuHCl concentrations, consistent with an intermediate with more compact structure at 1 M GuHCl.

Small-angle X-ray scattering (SAXS) was performed on SMA solutions to determine the molecular size and compactness during its unfolding. Unfortunately, the limited sensitivity of this technique precluded using the same low concentrations of SMA used in the preceding experiments. The much higher SMA concentration used in the SAXS experiments means that we are starting with the SMA dimer, rather than monomer (see below). Figure 1h shows the radius of gyration (R_g) of SMA (240 μM) in the presence of various concentrations of GuHCl in phosphate buffer at pH 7.4. The inset shows the Kratky plots for SMA in 0 and 2 M GuHCl (dotted line). The R_g of 18.9 ± 0.55 Å for the native state is consistent with the R_g value calculated for the native SMA dimer. The radius of gyration of SMA with 1 M GuHCl at 240 μM (18.7 ± 0.66 Å) is the same as that of the native one, indicating that the dimers are still present and that the protein maintains its native-like compactness under these conditions. However, the Rg of SMA with 2 M GuHCl jumped to 25.2 ± 1.59 Å, indicating either dissociation to monomers, or a more unfolded-like conformation, or both. If the protein dissociated without unfolding, the R_g should decrease. If it unfolded without dissociating, the Rg should be larger than 25 Å (probably ~40 Å). Thus, the results suggest simultaneous dissociation to monomers and partial unfolding. Increasing the concentration of GuHCl from 2 to 5 M had no effect on the R_g. The Kratky plot of SMA with 5 M GuHCl still shows a curve indicating a partially folded conformation (data not shown), presumably resulting from the intramolecular disulfide bridge, and perhaps the aromatic cluster.

Kinetics of SMA Fibrillation Starting from Different Partially Unfolded States. The kinetics of SMA fibrillation were monitored by following the increase in fluorescence intensity of ThT upon binding to fibrils (*8*). The kinetics of

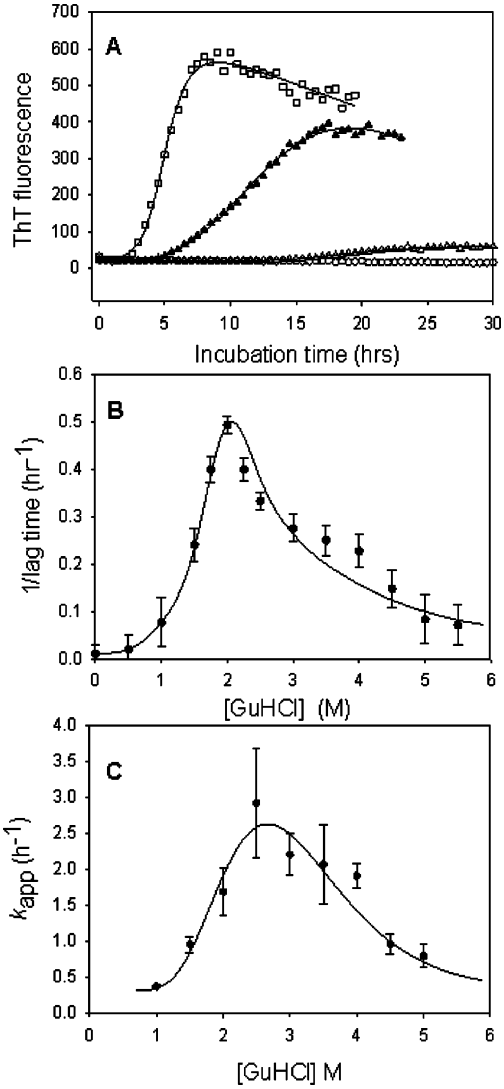

FIGURE 2: Kinetics of fibril formation of SMA at 40 μM, 37 °C, pH 7.4 (10 mM phosphate buffer, 200 mM NaCl), in the presence of various concentrations of GuHCl. (A) ThT fluorescence was used to monitor fibril formation at 0 M GuHCl (○); 1.5 M GuHCl (▲); 2 M GuHCl (□); and 5 M GuHCl (△). (B) Lag time of the fibril formation of SMA as a function of GuHCl concentration: Fibril formation kinetics were faster with increasing GuHCl concentrations to 2 M and then slowed down as the concentration of GuHCl increased further. (C) Elongation rate constants of SMA fibrillation in the presence of various concentrations of GuHCl.

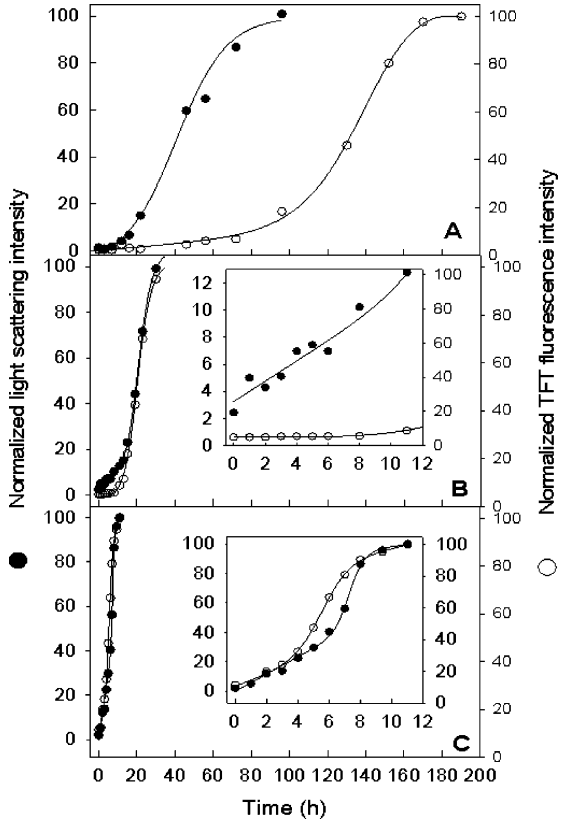

FIGURE 3: GuHCl concentration-dependence of SMA aggregation monitored by Rayleigh light scattering as well as ThT binding fluorescence. Concentration of SMA was 40 μM, at 37 °C, pH 7.4 (10 mM phosphate buffer, 200 mM NaCl). Rayleigh light scattering was used to monitor the formation of both amorphous (●) and fibrillar aggregations at 0 M GuHCl (A), 1.0 M GuHCl (B), and 2 M GuHCl (C). TFT fluorescence was used to monitor selectively fibril formation (○). The insets in panels B and C present the data of the first 12 h to show clearly the relationship between light scattering and TFT fluorescence.

fibrillation usually show a sigmoidal pattern, from which the lag time can be measured to indicate the time of nucleation (*26*) and in which the exponential increase of the transition represents the rate of fibril elongation. As shown in Figure 2A, the kinetics of SMA fibrillation were very dependent on the concentration of GuHCl. No increase in ThT fluorescence intensity was observed from SMA incubated under native conditions (pH 7.4, 0 M GuHCl) without agitation for 1 month, indicating that SMA forms fibrils very slowly under these conditions (data not shown). Even with the agitation as described in the methods section, the rate of fibrillation of SMA under native conditions was slow, with a lag time of 100 h. Upon increasing the concentration of GuHCl, the lag time decreased, and reached its shortest period at 2 M GuHCl (Figure 2B). This indicates that the partially folded intermediate populated at 2 M GuHCl has the highest propensity to form fibrils. With increasing concentrations of GuHCl above 2 M, the lag time increased, indicating a decreased nucleation rate, and reflecting the increased unfolding of the protein. The rate of fibril elongation with increasing GuHCl (Figure 2C) paralleled the changes in lag time, suggesting that the partially unfolded conformation of SMA, which was critical for formation of the nucleus, was also necessary for fibril elongation.

Since enhanced ThT fluorescence is relatively specific for fibrils, it is not a suitable probe for other types of aggregation of SMA. Consequently, we used Rayleigh light scattering to monitor total aggregation during the incubation of SMA. For SMA in its native state (10 mM phosphate buffer, pH 7.4), the light scattering intensity increased much more rapidly compared to the slow rate of fibrillation probed by ThT (lag time 100 h) indicating that non-fibrillar aggregates formed prior to fibrils (Figure 3). The maximum TFT signal for 1.0 M GuHCl was 40, and for 2 M GuHCl it was 300 arbitrary units. Electron microscope images of SMA aggregates at different stages of incubation under these conditions show that oligomers were formed in the early stage and were responsible for the increased light scattering without ThT fluorescence (Figure 4A). The increase in ThT fluorescence correlated with fibril formation as seen by EM (Figure 4B). In the presence of 1 M GuHCl, both light scattering and ThT fluorescence changes were accelerated, but the initial increase in light scattering intensity still

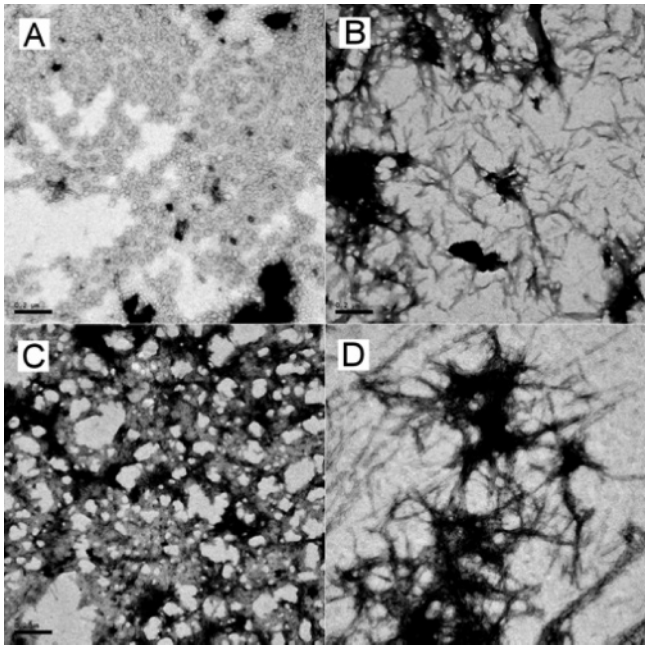

FIGURE 4: Transmission electron micrographs of SMA aggregates. (A) The oligomers present in the early stages of SMA aggregation, at 72 h of incubation at native state (0 M GuHCl, 10 mM phosphate buffer, pH 7.4), which showed increased light scattering intensity but no change of ThT fluorescence (Figure 3A). After 200 h of incubation, aggregates of fibrils were present in solution as shown in B. (C) The amorphous aggregates formed in the presence of 1 M GuHCl after being incubated 24 h, and (D) fibrils of SMA formed in the presence of 2 M GuHCl after incubation at 37 °C for 10 h.

occurred prior to the changes in ThT signal, indicating the formation of non-fibrillar aggregates prior to fibrils (Figure 3C). The EM images of the SMA aggregates taken from samples at late stages of incubation showed that SMA incubated in the presence of 1 M GuHCl (the native-like intermediate state) formed mostly amorphous aggregates with a few fibrils, responsible for the increased ThT signal. On increasing the concentration of GuHCl to 2 M, both the light scattering intensity and ThT fluorescence increased simultaneously with a lag time of 2 h (Figure 3C). The corresponding EM images indicated that the predominant aggregated species was fibrils (Figure 4D). Thus, at 2 M GuHCl essentially only fibrils were formed, in contrast to the situation at lower GuHCl concentrations, where amorphous deposit formation competed with fibrillation.

Association State of SMA. The dissociation constant for SMA dimers is in the μM range (*27*). In this study, we used near-UV CD, fluorescence anisotropy, and SAXS to monitor the association state of SMA as a function of its concentration in the presence of 2 M GuHCl. This concentration of GuHCl was chosen since it is optimal for SMA fibrillation under these conditions (see below).

Near-UV CD spectra of SMA with concentrations ranging from 0.8 to 240 μM were collected in the presence of 2 M GuHCl (Figure 5A, inset). From the dependence of ellipticity at 280 nm on the protein concentration, a dissociation constant of 102 ± 2 μM was determined (we have previously shown that the monomer/dimer equilibrium can be monitored by near-UV CD (*12*). This dissociation constant is larger than that of SMA under native state conditions, which was reported as 40 μM (*27*), indicating that, as anticipated, GuHCl destabilizes the dimer association.

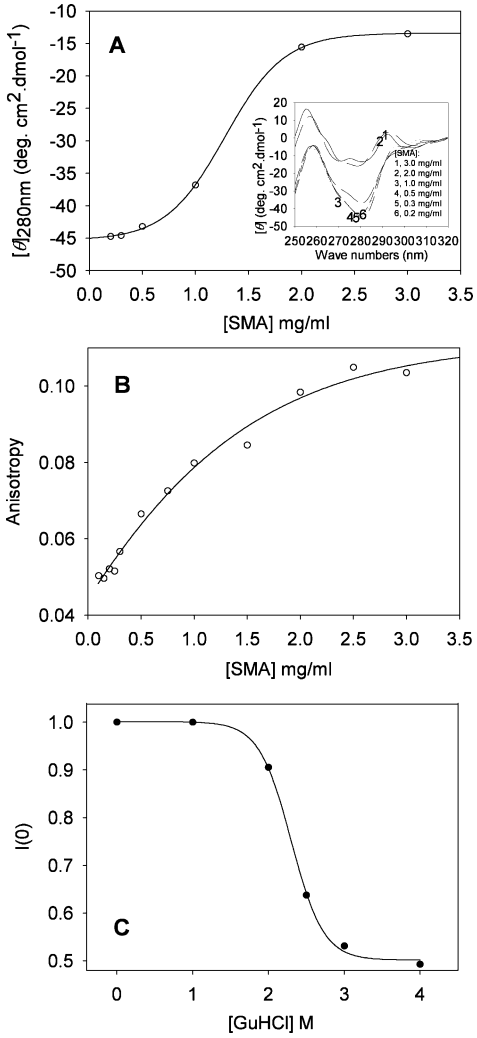

FIGURE 5: The association state of SMA as a function of GuHCl concentrations. (A) The transition curve of association of SMA with various concentrations in the presence of 2 M GuHCl monitored by near-UV circular dichroism. The insets are the near-UV spectra of SMA at the concentrations of 16, 24, 40, 80, 160, and 240 μM, respectively. (B) Anisotropy of SMA at various concentrations in the presence of 2 M GuHCl, showing the association of dimeric as the concentration of the protein increased. (c) Normalized/(0) values extrapolated from small angle x-ray scattering profiles of SMA solutions with a concentration of 240 μM at pH 7.5 (10 mM phosphate buffer with 200 mM NaCl) plotted as a function of GuHCl concentration. At the concentration of 240 μM SMA shows a dimeric state with the concentrations of GuHCl lower than 2 M, while the molecules disassociated into monomers at higher concentrations of GuHCl.

Fluorescence anisotropy of SMA was measured as a function of protein concentration in the presence of 2 M GuHCl. As shown in Figure 5B, the tryptophan fluorescence anisotropy increased with increasing concentration of the protein, coinciding with the increased population of dimers. The plot of anisotropy as a function of concentration gave a dissociation constant of 90 ± 11 μM, similar to the value determined from near-UV CD spectra. No significant differences in λ_{max} and concentration-normalized intensity of intrinsic fluorescence were observed (data not shown), indicating that the microenvironments of the two tryptophan residues were not significantly different between the monomeric and the dimeric forms of SMA.

The stabilities of monomer and dimer were investigated by GuHCl titration monitored by Trp fluorescence. At a

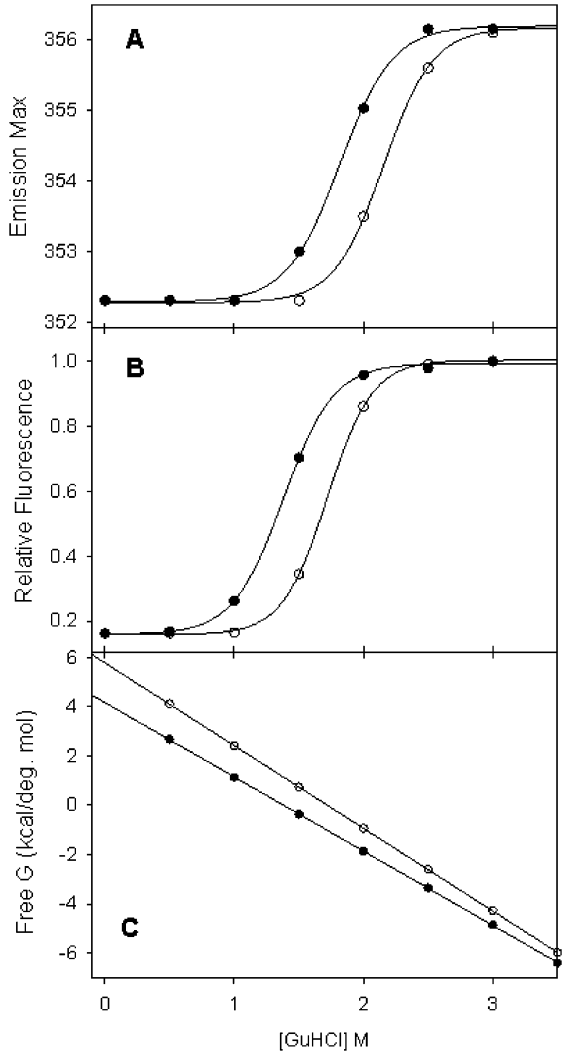

FIGURE 6: Stability of SMA at monomer/dimer states measured by GuHCl titration probed by intrinsic fluorescence. (A) Emission wavelengths of monomer (5 μM, ●) and dimer (240 μM, ○) against concentration of GuHCl. (B) Fluorescence intensity of monomer (5 μM, ●) and dimer (240 μM ○) against concentration of GuHCl. (C) The ΔG of monomer (5 μM, ●) and dimer (240 μM ○) extrapolated from Trp intrinsic fluorescence data of GuHCl titration.

protein concentration of 5 μM, where SMA was predominantly monomeric, the unfolding transition showed a C_m of 1.82 ± 0.02 M from λ_{max}, and 1.38 ± 0.01 M from fluorescence intensity, as shown in Figure 6A,B. Significantly, when the concentration of SMA was 180 μM, where SMA is predominantly dimeric, the midpoints of the unfolding transition for λ_{max} and fluorescence intensity shifted to higher concentrations of GuHCl, with values of 2.16 ± 0.01 M and 1.72 ± 0.01 M respectively. Values of $\Delta G(0)$, extrapolated from intrinsic Trp fluorescence (Figure 6C) demonstrated, as expected, that dimers of SMA were more stable: 4.17 and 5.78 kcal/mol for monomer and dimer, respectively. The steeper slope (higher *m* value) of the dimer is consistent with a greater increase in solvent-accessible surface area for the dimers compared to the monomers, as would be expected.

Effect of Association State on SMA Fibrillation. As shown above, SMA dimerizes with a dissociation constant of 100 μM in the presence of 2 M GuHCl. In order to clarify the effect of the association state on the fibrillation of SMA, the kinetics of SMA fibrillation were measured with various concentrations of protein in 2 M GuHCl. As shown in Figure 7, the length of the lag time decreased with the increasing concentration of SMA in the low concentration range ($\leq$50 μM), and then increased at higher concentrations, indicating that the dimer, which is present at the higher concentrations of protein, inhibited formation of the nucleation step of fibrillation. The rates of fibril elongation correlated with the lag times, suggesting that the associated state not only inhibited the nucleation process, but fibril elongation as well. Moreover, during the incubation of SMA at high concentration in the presence of 2 M GuHCl, no significant light scattering intensity changes were observed prior to the ThT fluorescence increase (data not shown), suggesting that no amorphous aggregation occurred prior to fibrillation. EM images show that the predominant insoluble species was fibrils at all SMA concentrations, indicating that the initial association state did not affect the partitioning between fibrillation and off-pathway amorphous aggregation.

To compare the effect of the different stabilities of the SMA monomer and dimer on fibrillation, the kinetics of SMA fibrillation at low (40 μM: monomer) and high concentration (240 μM: dimer) were measured at different concentrations of GuHCl. The maximum rate of fibrillation shifts from 2 M GuHCl for the monomer to 3 M for the dimer; conditions where the dimer significantly dissociates to monomer (Figure 7D). Combined with the stabilities of the monomer/dimer shown in Figure 6, this observation indicates that the dimer is more stable than monomer, and needs more destabilizing conditions to fibrillate. This corroborates that the monomeric state is required for fibrillation.

DISCUSSION

More and more secreted proteins have been found to have the potential to produce extracellular amyloid deposits in multiple organs (*28*). Although the characteristics of the soluble forms of these proteins are very varied—they range from intact globular proteins to largely unstructured peptide molecules—the aggregated forms have many characteristics in common (*29*). In addition to specific optical behavior (such as birefringence) on binding certain dye molecules (e.g., Congo red), the fibrillar structures typical of many of the aggregates have very similar morphologies (long, unbranched, and often twisted structures a few nanometers in diameter) and a common structural motif (consisting of cross-β-sheets in which the peptide strands are arranged perpendicular to the long axis of the fibrils). The ability of polypeptide chains to form amyloid structures is not restricted to the relatively small number of proteins associated with recognized clinical disorders. Recent data suggest that many soluble proteins can, under certain circumstances, undergo this conversion (*30*, *31*).

The immunoglobulin light chain variable domain consists of a highly conserved framework formed by two sheets of antiparallel β-strands forming a β-sandwich, and three loops comprising the complementarity-determining regions (CDR) that form part of the antigen binding site. As previously described (*12*−*14*), the light chain variable domain LEN, a benign (non-amyloidogenic) V_L, forms fibrils in vitro under mildly destabilizing conditions. The amyloidogenic V_L domain SMA is very homologous to LEN with sequence

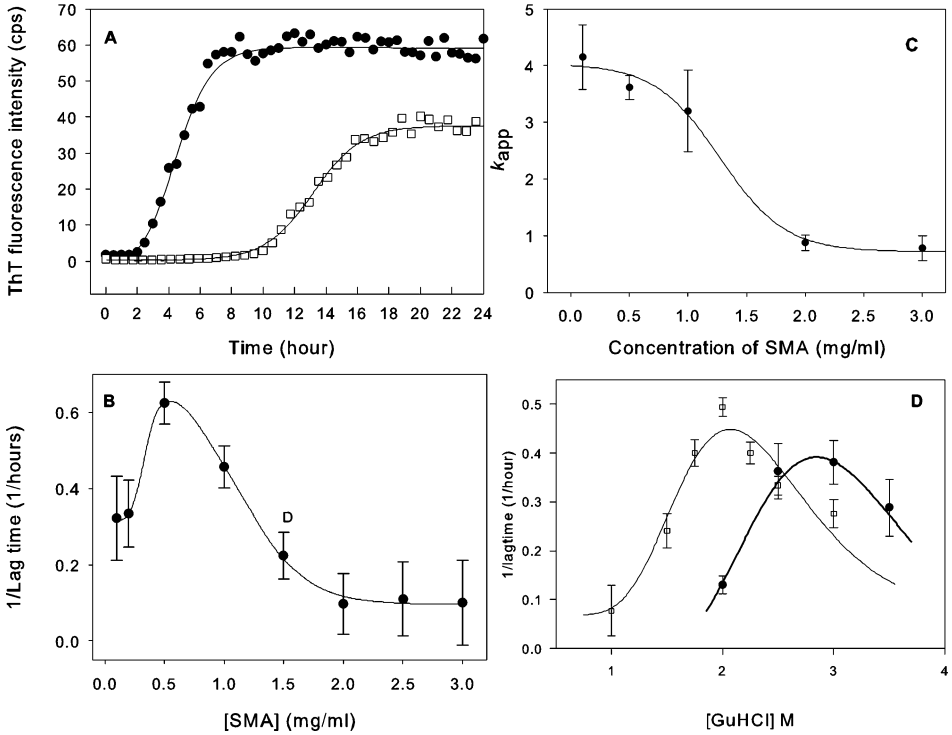

FIGURE 7: Effect of protein concentration on the fibrillation of SMA. (A) Kinetics of fibrillation of SMA in the presence of 2 M GuHCl, 37 °C, pH 7.4 (10 mm phosphate buffer, 200 mm NaCl), at concentrations of 40 μM (●) and 240 μM (□) probed by ThT fluorescence intensity. (B) Lag times of the fibril formation of SMA as a function of protein concentration. Fibril formation kinetics was faster with increasing SMA concentrations to 40 μM and then slowed down as the concentration of SMA further increased. (C) Elongation rate constants of SMA fibrillation at different protein concentrations in the presence of various concentrations of GuHCl. (D) Comparison of fibrillation rates between low (40 μM, □) and high (240 μM, ●) concentration of SMA in the presence of different concentrations at GuHCl.

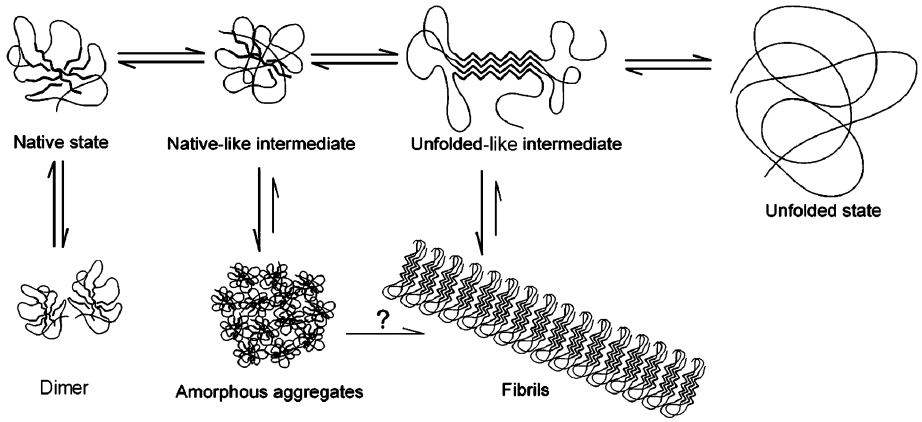

FIGURE 8: Proposed model for the light chain V_L domain SMA aggregation. The monomer (either native or unfolded) can form a native-like partially folded intermediate that preferentially forms amorphous aggregates and a more unfolded intermediate that preferentially forms fibrils. It is not clear whether molecules in the amorphous aggregates can convert to fibrils without prior dissociation to monomeric species.

differences mostly in the CDR loops. These observations suggest that environmental conditions may play a key role in leading to fibrils.

Destabilizing Conditions Promote Two Partially Folded Intermediates. Previously we showed that decreasing the pH leads to two partially folded intermediate conformations of SMA, I_N and I_U, the former being relatively native-like in its structural properties, whereas the latter is considerably more unfolded (*8*). In the present study, the effect of increasing concentrations of GuHCl on the conformation of SMA suggests that two comparable intermediates are formed, one at 1 M and the other at 2 M GuHCl. This means that destabilizing conditions in general will lead to these intermediates, with more strongly destabilizing conditions leading to the more unfolded intermediate that has a high propensity to form fibrils.

Properties of the Partially Folded Intermediates. The far-UV circular dichroism spectrum of the native state of SMA shows a negative ellipticity at 217 nm, representing its predominant β-structure. The extra minimum at 232 nm is due to the presence of aromatic clusters. In the presence of 1 M GuHCl, where the native-like intermediate conformation is maximally populated, the far-UV CD spectrum shows a similar shape to that of the native state, but with decreased ellipticity. Although this could be due to the loss of some secondary structure, it more likely represents changes in the aromatic cluster that contributes significantly to the spectrum. The near-UV CD spectrum indicates near-native-like tertiary

structure The near-UV circular dichroism, Trp fluorescence, fluorescence anisotropy and acrylamide quenching data all point to the compactness of the intermediate in 1 M GuHCl being similar to that of the native state. Thus, the intermediate populated in 1 M GuHCl appears to correspond to the previously detected I_N.

The data from biophysical analysis show that a more unfolded intermediate accumulated in the presence of 2 M GuHCl. The near-UV CD, Trp fluorescence, and SAXS data all point to the intermediate as having less tertiary structure. However, the enhanced negative ellipticity at 217 nm from far-UV CD spectrum indicates that more β-structure exists in this intermediate. The disappearance of the negative ellipticity of far-UV CD at 232 nm suggests that the aromatic clusters present in native conformation no longer exist. This was also confirmed by the near-UV CD spectrum, which indicates loss of most of the native aromatic interactions, but some remaining tertiary structure, presumably due to the presence of the disulphide bridge.

Only the Less-Structured Intermediate Leads to Fibril Formation. Although SMA formed amyloid in vivo, in vitro studies show that SMA solutions do not form fibrils under physiological condition for several months without agitation. However, if the sample is agitated by stirring or shaking, it forms fibrils with a lag time of about 100 h, but also is accompanied by amorphous deposits. On the basis of the fact that in the presence of 1 M GuHCl SMA rapidly forms amorphous aggregates and with 2 M GuHCl fibrils are formed rapidly, whereas under these conditions the predominant species are the native-like intermediate and more unfolded intermediate, respectively, we conclude that the more native-like intermediate preferentially leads to amorphous aggregates, whereas the more unfolded intermediate preferentially leads to fibrils. This can be accounted for by the need for significant flexibility in the molecule to allow for the necessary topological changes required to form the cross-beta structure of the fibrils. Figure 8 shows the minimum kinetic model to account for the aggregation/fibrillation properties of SMA.

Dimerization Inhibits Fibrillation. SMA has a significant propensity to self-associate to form dimers, with a dissociation constant of about 40 μM; this reflects the strong structural homology between light and heavy chain variable domains, which form a tight dimer. In the presence of 2 M GuHCl, the SMA dimer is destabilized and the disassociation constant shifted to 90−100 μM: thus SMA is mostly dimeric at 240 μM in the presence of 2 M GuHCl (Figure 4). Interestingly, the kinetics of SMA fibrillation showed that the rate of fibrillation was inversely dependent on the protein concentration (at higher concentrations): in contrast to most amyloid systems, the kinetics of SMA fibrillation became slower with increasing SMA concentrations (Figure 7). This suggests that dimerization inhibits the fibrillation. As described above, SMA fibrillation arises from a partially unfolded state; thus any factors that stabilize the native conformation could inhibit fibrillation. The data from the GuHCl-titration of both monomer and dimer clearly show that the dimer is more stable than monomer. Furthermore, the kinetics of SMA fibrillation for monomer and dimer show that the GuHCl concentration that is most favorable for the monomer fibrillation (2 M) shifts to 3 M for the dimer. Consequently, the greater stability of the dimer, by decreasing the amount of unfolded intermediate, inhibits the formation of fibrils.

ACKNOWLEDGMENT

Small-angle X-ray scattering measurements were performed on Beam line 4-2 at the Stanford Synchrotron Radiation Laboratory (SSRL).

REFERENCES

1. Sipe, J. D. (1992) Amyloidosis, *Ann. Rev. Biochem. 61*, 947−975.
2. Glenner, G. G. (1980) Amyloid deposits and amyloidosis. The beta-fibrilloses (first of two parts), *N. Engl. J. Med. 302*, 1283−1292.
3. Gallo, G., Picken, M., Buxbaum, J., and Frangione, B. (1989) The spectrum of monoclonal immunoglobulin deposition disease associated with immunocytic dyscrasias, *Semin. Hematol. 26*, 234−245.
4. Gallo, G., Goni, F., Boctor, F., Vidal, R., Kumar, A., Stevens, F. J., Frangione, B., and Ghiso, J. (1996) Light chain cardiomyopathy. Structural analysis of the light chain tissue deposits, *Am. J. Pathol. 148*, 1397−1406.
5. Stokes, M. B., Jagirdar, J., Burchstin, O., Kornacki, S., Kumar, A., and Gallo, G. (1997) Nodular pulmonary immunoglobulin light chain deposits with coexistent amyloid and nonamyloid features in an HIV-infected patient, *Mod. Pathol. 10*, 1059−1065.
6. Schormann, N., Murrell, J. R., Liepnieks, J. J., and Benson, M. D. (1995) Tertiary structure of an amyloid immunoglobulin light chain protein a proposed model for amyloid fibril formation, *Proc. Natl. Acad. Sci. U.S.A. 92*, 9490−9494.
7. Stevens, F. J., Myatt, E. A., Chang, C. H., Westholm, F. A., Eulitz, M., Weiss, D. T., Murphy, C., Solomon, A., and Schiffer, M. (1995) A molecular model for self-assembly of amyloid fibrils: immunoglobulin light chains, *Biochemistry 34*, 10697−10702.
8. Khurana, R., Gillespie, J. R., Talapatra, A., Minert, L. J., Ionescu-Zanetti, C., Millett, I., and Fink, A. L. (2001) Partially folded intermediates as critical precursors of light chain amyloid fibrils and amorphous aggregates, *Biochemistry 40*, 3525−3535.
9. Kim, Y., Wall, J. S., Meyer, J., Murphy, C., Randolph, T. W., Manning, M. C., Solomon, A., and Carpenter, J. F. (2000) Thermodynamic modulation of light chain amyloid fibril formation, *J. Biol. Chem. 275*, 1570−1574.
10. Wall, J., Schell, M., Murphy, C., Hrncic, R., Stevens, F. J., and Solomon, A. (1999) Thermodynamic instability of human lambda 6 light chains: correlation with fibrillogenicity, *Biochemistry 38*, 14101−14108.
11. Khurana, R., Souillac, P. O., Coats, A. C., Minert, L., Ionescu-Zanetti, C., Carter, S. A., Solomon, A., and Fink, A. L. (2003) A model for amyloid fibril formation in immunoglobulin light chains based on comparison of amyloidogenic and benign proteins and specific antibody binding, *Amyloid 10*, 97−109.
12. Souillac, P. O., Uversky, V. N., Millett, I. S., Khurana, R., Doniach, S., and Fink, A. L. (2002) Effect of association state and conformational stability on the kinetics of immunoglobulin light chain amyloid fibril formation at physiological pH, *J. Biol. Chem. 277*, 12657−12665.
13. Souillac, P. O., Uversky, V. N., Millett, I. S., Khurana, R., Doniach, S., and Fink, A. L. (2002) Elucidation of the molecular mechanism during the early events in immunoglobulin light chain amyloid fibrillation: Evidence for an off-pathway oligomer at acidic pH, *J. Biol. Chem. 277*, 12666−12669.
14. Souillac, P. O., Uversky, V. N., and Fink, A. L. (2003) Structural Transformations of oligomeric intermediates in the fibrillation of the immunoglobulin light chain LEN, *Biochemistry 42*, 8094−8104.
15. Teng, J., Russell, W. J., Gu, X., Cardelli, J., Jones, M. L., and Herrera, G. A. (2004) Different types of glomerulopathic light chains interact with mesangial cells using a common receptor but exhibit different intracellular trafficking patterns, *Lab. Invest. 84*, 440−451.
16. Stevens, P. W., Raffen, R., Hanson, D. K., Deng, Y. L., Berrios-Hammond, M., Westholm, F. A., Murphy, C., Eulitz, M., Wetzel, R., Solomon, A., Schiffer, M., and Stevens, F. J. (1995) Recombinant immunoglobulin variable domains generated from

synthetic genes provide a system for in vitro characterization of light-chain amyloid proteins, *Protein Sci. 4*, 421−432.
17. Pras, M., Schubert, M., Zucker-Franklin, D., Rimon, A., and Franklin, E. C. (1968) The characterization of soluble amyloid prepared in water, *J. Clin. Invest. 47*, 924−933.
18. Solomon, A. (1985) Light chains of human immunoglobulins, *Methods Enzymol. 116*, 101−121.
19. Huang, D. B., Chang, C. H., Ainsworth, C., Johnson, G., Solomon, A., Stevens, F. J., and Schiffer, M. (1997) Variable domain structure of kappaIV human light chain Len: high homology to the murine light chain McPC603, *Mol. Immunol. 34*, 1291−1301.
20. Uversky, V. N., Karnoup, A. S., Khurana, R., Segel, D. J., Doniach, S., and Fink, A. L. (1999) Association of partially-folded intermediates of staphylococcal nuclease induces structure and stability, *Protein Sci. 8*, 161−173.
21. Guinier, A., and Fournet, G. (1955) Small-angle scattering of X-rays, in *Small-Angle Scattering of X-rays*; *Structure of Matter* Series, pp 268, Wiley, New York.
22. Sreerama, N., Venyaminov, S. Y., and Woody, R. W. (1999) Estimation of the number of alpha-helical and beta-strand segments in proteins using circular dichroism spectroscopy, *Protein Sci. 8*, 370−380.
23. Fink, A. L. (1999) ANS, in *The Encyclopedia of Molecular Biology* (Creighton, T. E., Ed.) pp 140−142, John Wiley & Sons, New York.
24. Semisotnov, G. V., Rodionova, N. A., Razgulyaev, O. I., Uversky, V. N., Gripas', A. F., and Gilmanshin, R. I. (1991) Study of the "molten globule" intermediate state in protein folding by a hydrophobic fluorescent probe, *Biopolymers 31*, 119−128.
25. Stryer, L. (1968) Fluorescence spectroscopy of proteins, *Science 162*, 526−533.
26. Jarrett, J. T., and Lansbury, P. T., Jr. (1992) Amyloid fibril formation requires a chemically discriminating nucleation event: studies of an amyloidogenic sequence from the bacterial protein OsmB, *Biochemistry 31*, 12345−12352.
27. Kolmar, H., Frisch, C., Kleemann, G., Gotze, K., Stevens, F. J., and Fritz, H. J. (1994) Dimerization of Bence Jones proteins: linking the rate of transcription from an Escherichia coli promoter to the association constant of REIV, *Biol. Chem. Hoppe Seyler 375*, 61−70.
28. Selkoe, D. J. (2003) Folding proteins in fatal ways, *Nature 426*, 900−904.
29. Sunde, M. and Blake, C. (1997) The structure of amyloid fibrils by electron microscopy and X-ray diffraction, *Adv. Protein Chem. 50*, 123−159.
30. Dobson, C. M. (1999) Protein misfolding, evolution and disease, *Trends Biochem. Sci. 24*, 329−332.
31. Dobson, C. M. (2001) The structural basis of protein folding and its links with human disease Philos, *Trans. R. Soc. Lond B. Biol. Sci. 356*, 133−145.

BI061716V